Web buckling analysis of steel-concrete composite beams considering flange restraints

Authors:

Qifeng Chen, MCE
Guangxi University of Science and Technology, Liuzhou, China
College of Civil and Architectural Engineering
Guangxi Beitou Traffic Maintenance Technology Group Co., Nanning, China
Chenqifeng3333@163.com

Zhiyao Hou, MCE
Guangxi Beitou Traffic Maintenance Technology Group Co., Nanning, China
hzy@my.swjtu.edu.cn
Corresponding author

Tianzhi Hao, MCE
Guangxi Beitou Traffic Maintenance Technology Group Co., Nanning, China
haotz@bgigc.com

Jiejun Ning, MCE
Guangxi Beitou Traffic Maintenance Technology Group Co., Nanning, China
417971615@qq.com

Research Paper

Qifeng Chen, Zhiyao Hou, Tianzhi Hao, Jiejun Ning

Web buckling analysis of steel-concrete composite beams considering flange restraints

A mechanical model was established to study the buckling of the web of steel-concrete composite beams under flange restraint. Based on the Rayleigh-Ritz variational methodology and elastic buckling theory, a theoretical buckling calculation model for steel-concrete composite beams with webs restrained by flanges was proposed. Through a parameter analysis, the variation in the web buckling coefficient with the rotational restraint coefficient of steel-concrete composite beams under different web aspect ratios and stress gradients was studied. The calculation accuracy of the proposed theoretical model was verified by comparing the calculation results under different parameters with those of a traditional model. Finally, considering the different distributions of the shear studs, the theoretical model proposed in this study was verified using the finite element method. The following results were obtained: the deviation between the theoretical model and the traditional model was less than 3 %, when the spacing of shear studs increased from 100 to 1000 mm, the critical buckling stress calculated by finite element method decreased from 121.90 to 113.29 MPa, with a deviation of less than 6 % from the theoretical model in this paper, both the theoretical model and the finite element calculation show that when the elastic restraint coefficient was greater than 20, the buckling coefficient region was constant.

Key words:
steel-concrete composite girders, shear studs, buckling, rotational restraints, web plates, steel-concrete composite flanges, critical stresses

Prethodno priopćenje

Qifeng Chen, Zhiyao Hou, Tianzhi Hao, Jiejun Ning

Analiza izbočenja hrpta spregnutih nosača čelik-beton s obzirom na pridržanja pojasnicom

Utvrđen je mehanički model za proučavanje izbočenja hrpta spregnutih nosača čelik-beton pod utjecajem pridržanja pojasnicom. Primjenom Rayleigh-Ritzove varijacijske metode i elastične teorije izbočenja predložen je teorijski model izračuna izbočenja za spregnute nosače čelik-beton s hrptovima pridržanima pojasnicama. Analizom parametara ispitana su odstupanja koeficijenta izbočenja hrpta s koeficijentom rotacijskog pridržanja spregnutih nosača čelik-beton pri različitim omjerima širine i gradijentima naprezanja. Točnost izračuna predloženog teorijskog modela provjerena je usporedbom rezultata izračuna pri različitim parametrima s rezultatima tradicionalnog modela. Naposljetku, s obzirom na različite raspodjele moždanika, teorijski model predložen u ovome istraživanju potvrđen je metodom konačnih elemenata. Dobiveni su sljedeći rezultati: odstupanje između teorijskog modela i tradicionalnog modela bilo je manje od 3 %, nakon što se razmak moždanika povećao sa 100 na 1000 mm, kritično naprezanje izbočenja izračunano metodom konačnih elemenata smanjilo se sa 121,90 na 113,29 MPa, uz odstupanje manje od 6 % od teorijskog modela u ovome radu i teorijski model i izračun metodom konačnih elemenata pokazuju to da kada se koeficijent elastičnog pridržanja bio veći od 20, područje koeficijenta izbočenja nije se smanjivalo.

Ključne riječi:
spregnuti nosači čelik-beton, moždanici, izbočenje, rotacijsko pridržanje, hrbat, spregnute pojasnice čelik-beton, kritična naprezanja

1. Introduction

Steel-concrete composite girders have been extensively used in long-span bridge engineering in recent years. This type of composite member combines the benefits of high integral rigidity, light weight, and a large span capacity. However, the depth to thickness ratio of the web plates used in these composite girders is large, and the slender designs have resulted in a tendency towards local buckling. This situation makes it imperative to accurately assess the elastic critical buckling factor to avoid local buckling while optimising the web design. Traditionally, elastic buckling in steel plates was determined by assuming that the web plates were simply supported at the junctions between the flanges and the web. Most studies have been based on this assumption [1-4]; they used the energy method, experimental method, and finite element method (FEM) to analyse the plate buckling behaviours related to bending and shear stresses. For example, after assigning constraints to the EBPlate software, the buckling behaviour of the web plate can be analysed using the Rayleigh–Ritz Variational method [5]. The results are conservative because the elastic rotational restraints of the flanges are ignored. Moreover, the results are more conservative for composite girders because the rotational restraint coefficients are larger for steel-concrete composite flanges. Estrada et al. [6, 7] reported that the shear buckling coefficients of real boundary conditions were between those of simply supported and fixed-support conditions. Keerthan [8] and Bedair [9] also indicated that the conservative web panel boundary conditions were not sufficiently precise; thus, the effects of the true support conditions at the juncture between the flange and web must be considered.

To consider the rotational restraint of flanges, Qiao used combined harmonic and polynomial buckling deformation functions and the Ritz energy method [10, 11] to derive an orthotropic plate critical buckling stress formula under axial compression and shear. Pham analysed the shear buckling characteristics of the web in thin-walled channel section girders [12], where the critical buckling stress of the web increased as the rotational rigidity of the flanges increased. Keerthan researched the elastic buckling of webs under shear for LiteSteel beams [8], and the results indicated that the web buckling coefficient was between the coefficients for simple-supported and fixed-supported boundary conditions. László derived an explicit mathematical formulation for the plate with rotationally restrained longitudinal edges. Chen Liang [13] considered the case of two-step arrangement of shear studs, derived the relationship between mid-span deflection and interface stiffness, and obtained a deflection calculation method for composite beams based on threshold interface shear stiffness under ultimate state. Alexandre Rossi [14], Krzysztof Ś ledziewski [15], W.M.A.D. Wijethunter [16] and others used finite element method to study the lateral buckling of steel-concrete composite structures but did not consider the influence of shear nail arrangement. Araujo [17] studied the lateral buckling of steel-concrete composite structures based

on kinematics and mechanics and derived an analytical formula for calculating the buckling of simply supported I-beams constrained by concrete. However, the formula did not consider the influence of the shear nail distribution. Numerous studies have been devoted to the performance of web buckling [18, 19], or on how the rotational restraint of boundaries affects the buckling mode of the web; however, no information is available thus far on how steel-concrete composite girder flanges affect the buckling coefficient of the web, and how the concrete deck and shear studs impact the buckling coefficient is still unknown. In this study, a theoretical model was developed to study the local buckling of a composite girder web with elastically restrained edges subjected to uneven in-plane pressure. The Ritz energy variation method was utilised as a theoretical solution formula for uneven pressures to calculate the critical buckling coefficient of the web. Subsequently, based on the elastic theory of plates, the elastic restraint coefficients of steel-concrete composite flanges with different shear stud distributions were derived. Finally, a Finite Element Model (FEM) of a steel-concrete composite I-beam girder segment is established to verify the accuracy of the formula.

2. Local buckling formulation for a restrained web

This section presents the local buckling formulation for a web with a composite girder subjected to uneven in-plane axial loads along simply supported edges. A mechanical analysis model was established as shown in Figure. 1. In this model, because the rotational rigidity of the transverse stiffener is much less than that of the flanges, the web of the composite girder and the boundary conditions can be simplified to consist of a rectangular plate with the right and left edges simply supported and the top and bottom edges rotationally restrained [10].
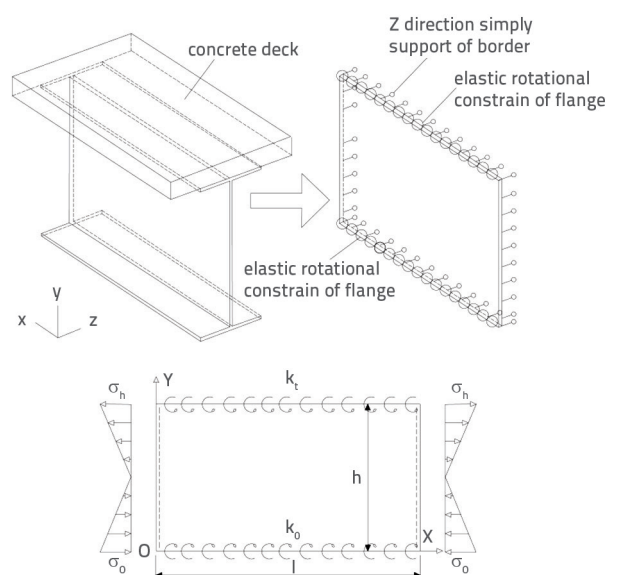

Figure 1. Mechanical analysis model of a web in a steel-concrete composite girder

In this study, U denotes the elastic strain energy stored in the web, U_{brou} denotes the strain energy stored in the rotationally restrained boundaries of the web, V_b denotes the work done by the uneven axial forces, and w denotes the buckling displacement. Based on the Rayleigh–Ritz Variational method, the displacement function selected for the elastic buckling deformation of webs with rotationally restrained boundaries is expressed as

$$w(x,y) = \left[\frac{y}{h} + w_1\left(1 - \cos\frac{\pi y}{h}\right) + w_2\left(\frac{y}{h}\right)^3 + w_3\left(\frac{y}{h}\right)^4 \right]$$
$$\times \sum_{m=1}^{\infty} \alpha_m \sin\left(\frac{m\pi x}{l}\right) \tag{1}$$

where w_1, w_2, and w_3 are unknown constants that can be determined by the boundary conditions, h is the height of the web plate, l is the width of the web plate, and m is an undetermined coefficient. The boundary conditions for the rotationally restrained edges shown in Figure 1 are expressed as follows:

$$w(x,0) = 0; w(x,h) = 0 \tag{2}$$

$$-D\left(\frac{\partial^2 w}{\partial y^2} = v\frac{\partial^2 w}{\partial x^2}\right) = C_0 \frac{\partial^3 w}{\partial x^2 \partial y}_{,y=0}$$
$$-D\left(\frac{\partial^2 w}{\partial y^2} = v\frac{\partial^2 w}{\partial x^2}\right) = C_t \frac{\partial^3 w}{\partial x^2 \partial y}_{,y=h} \tag{3}$$

$$C_0 = GJ_s = G\sum \frac{1}{3}m_i t_i^3$$
$$C_t = GJ_s = G\sum \frac{1}{3}m_i t_i^3 \tag{4}$$

where C_0 and C_t are the torsional rigidities of the upper and lower flanges, respectively; m_i is the width of the flange plate; t_i is the thickness of the flange; G is the shear modulus of the steel; and D is the web bending stiffness coefficient. Substituting the results of Eq. (1) into Eq. (3), Eq. (3) can be approximated as follows:

$$D\frac{\partial^2 w}{\partial y^2} \approx k_0 \frac{\partial w}{\partial y}_{,y=0}$$
$$D\frac{\partial^2 w}{\partial y^2} \approx k_t \frac{\partial w}{\partial y}_{,y=h} \tag{5}$$

where k_0 and k_t denote the elastic rotational constraint stiffnesses of the lower and upper flanges, respectively [20], and can be expressed as

$$k_0 = \pi^2 C_0 / l^2, k_t = \pi^2 C_t / l^2 \tag{6}$$

Substituting the results of Eq. (1) into Eqs. (2) and (5), the unknown constants of the displacement function that satisfy all boundary conditions can be solved as follows:

$$w_1 = \frac{X_0}{\pi^2} \tag{7}$$

$$w_2 = \frac{12\pi^2 + 24X_0 + \pi^2 X_0 - 3\pi^2 X_t - 8X_0 X_t}{\pi^2(X_t - 6)}$$
$$w_3 = -\frac{6\pi^2 + 12X_0 + \pi^2 X_0 - 2\pi^2 X_t - 6X_0 X_t}{\pi^2(X_t - 6)} \tag{7}$$

where χ_0 and χ_t are the elastic restraint coefficients of the upper and lower flanges respectively [10, 20], which is expressed as:

$$X_0 = k_0 h/D, X_t = k_t h/D \tag{8}$$

Based on the Ritz Energy Method, the elastic strain energy of web U is expressed as

$$U = \frac{D}{2}\int_0^h \int_0^l \left\{ \begin{array}{c} \left(\frac{\partial^2 w}{\partial x^2}\right)^2 + 2v\left(\frac{\partial^2 w}{\partial x^2}\frac{\partial^2 w}{\partial y^2}\right) + \\ 2(1-v)\left(\frac{\partial^2 w}{\partial y \partial x}\right)^2 + \left(\frac{\partial^2 w}{\partial y^2}\right)^2 \end{array} \right\} dxdy \tag{9}$$

where v is the Poisson's ratio. The strain energy U_{brou} stored in the boundary equivalent spring is expressed as follows:

$$U_{brou} = \frac{1}{2}\int_0^1 \left[k_0\left(\frac{\partial w}{\partial x}_{,y=0}\right)^2 + k_t\left(\frac{\partial w}{\partial x}_{,y=h}\right)^2 \right] dx \tag{10}$$

The work V_b performed by in-plane uneven loads can be expressed as

$$V_b = -\frac{\sigma_0 t}{2}\int_0^h \int_0^l \left(\frac{\partial w}{\partial x}\right)\left(1 - \lambda\frac{y}{h}\right)dxdy \tag{11}$$

where, $\sigma = (\sigma_0 - \sigma_t) = \sigma_0$, is the in-plane load gradient coefficient of the uneven distribution of the load, and σ_0 and σ_t are defined as the stress at the point of $y = 0$ and h. According to the law of energy conservation, the variational form of the total potential energy of a web is expressed by Eq. (12):

$$\delta\prod = \delta U + \delta U_{brou} - \delta V_b = 0 \tag{12}$$

Because the variation m is arbitrary [10], i linear equations can be found in Eq. (13). The eigenvalue of i linear equation can be solved using Eq. (14).

$$K_{ij}\alpha_j = 0 \tag{13}$$

$$|K_{ij}| = 0 \tag{14}$$

Substituting the results of Eq. (1) into Eqs. (12) and (14), a variational form of the elastic strain energy stored in web U, the strain energy stored in the rotationally restrained boundaries of web U_{brou}, and the work done by the uneven axial force V_b can be respectively solved as:

$$\delta U = \begin{bmatrix} \dfrac{D\pi^4 h}{5040 l^3} A_1 \sum_{m=1}^{\infty} \alpha_m m^4 \delta\alpha_m + \dfrac{Dl}{4h^3} A_2 \sum_{m=1}^{\infty} \alpha_m \delta\alpha_m - \\[2ex] \dfrac{Dv\pi^2}{2hl} A_3 \sum_{m=1}^{\infty} \alpha_m m^2 \delta\alpha_m + \dfrac{D(1-v)\pi^2}{210hl} A_6 \sum_{m=1}^{\infty} \alpha_m m^2 \delta\alpha_m \end{bmatrix}$$ (15)

$$\delta V_b = -\frac{\sigma th\pi^2}{10080 l} A_7 \sum_{m=1}^{\infty} \alpha_m m^2 \delta\alpha_m$$

$$\delta U_{brou} = \frac{lD}{4h^3} A_4 \sum_{m=1}^{\infty} \alpha_m \delta\alpha_m$$

Detailed expressions for A_1, A_2, A_3, A_4, A_6, A_7 are provided in Table 1. By substituting A_1, A_2, A_3, A_4, A_6, A_7 into Eq. 15, the solution of the webs' first eigenvalue can be obtained, and the critical local buckling coefficient can be expressed as:

$$k_b = -\frac{10080}{A_7 \pi^4} \left(\frac{\pi^4 m^2}{5040 \gamma^2} A_1 + \frac{\gamma^2}{40m^2} A_2 + \frac{v\pi^2}{140} A_3 + \frac{(1-v)\pi^2}{140} A_6 + \frac{\gamma^2}{4m^2} A_4 \right)$$ (16)

where, $\gamma = l/h$ is the aspect ratio of the web. The critical buckling stress of the web can be expressed as follows:

$$\sigma_{cr} = \frac{k_b \pi^2 D}{h^2 t}$$ (17)

Table 1. Expressions for A_1, A_2, A_3, A_4, A_6, A_7 given in Eq. (15)

$$A_1 = \begin{Bmatrix} -30240\omega_1(\omega_2 + 2\omega_3) + 2520\pi^2\omega_1(2 + 3\omega_2 + 4\omega_3) \\[1ex] +\pi^4 \begin{bmatrix} 1890\omega_1^2 + 180\omega_2^2 + 126\omega_1(10 + 5\omega_2 + 4\omega_3) \\ +63\omega_2(8 + 5\omega_3) + 140(3 + 3\omega_3 + \omega_3^2) \end{bmatrix} \end{Bmatrix}$$

$$A_2 = \begin{bmatrix} 5\pi^2\omega_1^2 + 120\omega_2^2 + 360\omega_2\omega_3 \\ +288\omega_3^2 - 240(\omega_2 + 2\omega_3) \end{bmatrix}$$

$$A_3 = \begin{bmatrix} -35\pi^4\omega_1 + 1680\omega_1(\omega_2 + 2\omega_3) + 210\pi^2\omega_2\omega_3 \\ 2\pi^2(-70\omega_1 + 42\omega_2^2 + 70\omega_2 + 105\omega_3 + 60\omega_3^2) \end{bmatrix}$$

$$A_4 = \begin{bmatrix} X_0 + X_t(1 + 3w_2 + 4w_3)^2 \end{bmatrix}$$

$$A_6 = \begin{bmatrix} 35\pi^4\omega_1 - 1680\omega_1(\omega_2 + 2\omega_3) + 2\pi^2(70\omega_2 + 80\omega_3^2 + 140\omega_1) + \\ 2\pi^2(35 + 63\omega_2^2 + 70\omega_3 + 140\omega_1\omega_3 + 210\omega_1\omega_2 + 280\omega_1\omega_3) \end{bmatrix}$$

$$A_7 = \begin{Bmatrix} 5040\omega_1[-2 - 3\omega_2 + 4\omega_3 + \lambda(2 + 2\omega_1 + 4\omega_2 + 5\omega_3)] / \pi^2 - \\ 60480\omega_1[\omega_2(2\lambda - 1) + \omega_3(5\lambda - 2)] / \pi^4 + 129600\omega_1\omega_2\lambda / \pi^6 \\ -280[3 + \omega_3(3 + \omega_3)] + 1890\omega_1^2(\lambda - 2) + 36\lambda\omega_3(20 + 7\omega_3) \\ +45\omega_2^2(7\lambda - 8) + 84\omega_1[-6(5 + 2\omega_3) + 3\omega_3(4\lambda - 5)] + 590\lambda \\ +14\omega_2[-72 + 60\lambda + 5\omega_3(8\lambda - 9)] + 840\omega_1(2 + \omega_3)\lambda \end{Bmatrix}\pi^6$$

3. Coefficient of the web plate that was rotationally restrained

Based on the Rayleigh–Ritz Variational method, a critical buckling coefficient expression for a web rotationally restrained on the upper and lower flanges was derived using Eq. (16). While elastic restraint

coefficients, χ_0 and χ_t, provided for the upper and lower flanges in the composite girder were still uncertain, that problem was resolved in this section. Notably, the solutions provided in this section can only be used in the final state, where the concrete flange is solid and cannot consider the situation during the construction phase when the concrete is not solid. First, the boundary conditions of the web in the I-section girder along the flange-web joint connections are discussed, and then the coefficient of the rotationally restrained web in the I-section steel-concrete composite girder is analysed. According to the work done by Qiao [10], the boundary conditions of a web with steel girders can be simplified, as shown in Figure 2. The edges of the web-flange joint connections were simplified as elastic and rotationally restrained, whereas the torsional rigidity of the transverse stiffeners was much less than that of the flanges, and the left and right edges of the web could be simplified as simply supported edges.

Timoshenko [20] showed that as the web and flange plate connect (Figure 3), when buckling occurs, the rotational angle of the flange should be $\partial w/\partial g$, the rate of change in the rotation angle along the girder should be $\partial^2 w/\partial g\partial x$, and the torsional moment rate of change in the unit length along the *x-axis* in any cross-section of the upper and lower flanges can be expressed as follows:

$$C_t \frac{\partial^2 w}{\partial x \partial y}_{,y=h}, C_0 \frac{\partial^2 w}{\partial x \partial y}_{,y=0}$$ (18)
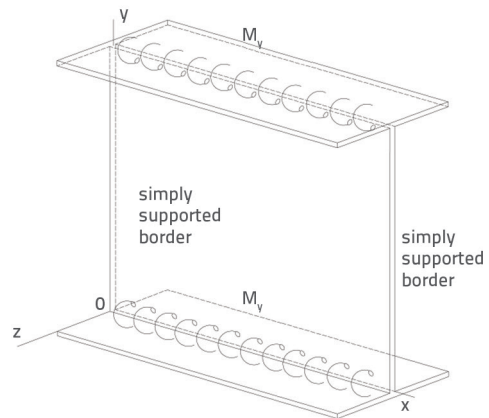

Figure 2. Boundary simplification of the web in the I-beam segment
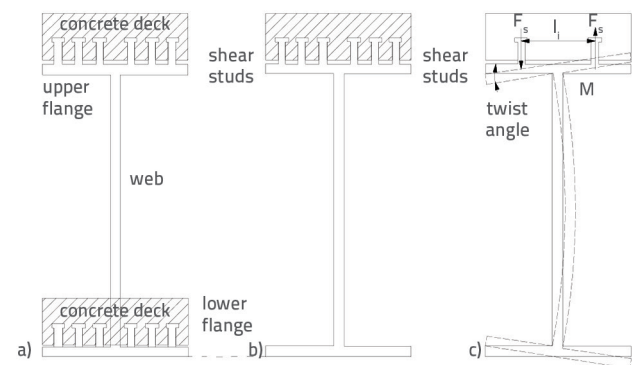

Figure 3. Mechanical analysis of shear studs in steel-concrete comp; b) concrete deck on the upper flange; c) simplified model

From the compatibility conditions of a web with flanges, the web unit length bending moment (along the flange-web joint connections) should be equal to the torsional moment rate of change in the unit length of the upper and lower flanges, and the boundary conditions of the web upper and lower edges can be referred to as Eqs. (3) and (5). As the steel flange and concrete deck of the combination flange are connected by shear studs, the torsional stiffness (C_z) of the combination flange can be expressed as

$$C_z = \min\{C_c, C_s\} + C_t \tag{19}$$

where C_c denotes the torsional rigidity of the concrete deck, C_s the torsional rigidity provided by the shear studs, and C_0 the torsional rigidity of the steel flange. The concrete-steel combination flanges twisted when web buckling occurred. As with a pair of symmetrical shear studs, there is pressure on one side of the shear stud, and tension on the other side, as shown in Figure 3, where the bending moment M_y along the sides of the upper and lower flanges of the web is proportional to the twist angle $\partial w / \partial g$, and the internal force of the shear studs F_s must be coordinated with the stress–strain relationship of the shear studs. Thus, the resisting bending moment, M_{s0}, provided by each pair of shear studs is:

$$M_{so} = F_s L_i = \frac{EAl_i^2}{2} \frac{\partial w}{\partial y} \tag{20}$$

Assuming that there are no rows of shear studs on one side of the web, as shown in Figure 4, the resisting bending moment M_{S1} provided by a column of shear studs is

$$M_{S1} = \sum_{i=1}^{n} \frac{EAl_i^2}{2} \frac{\partial w}{\partial y} \tag{21}$$
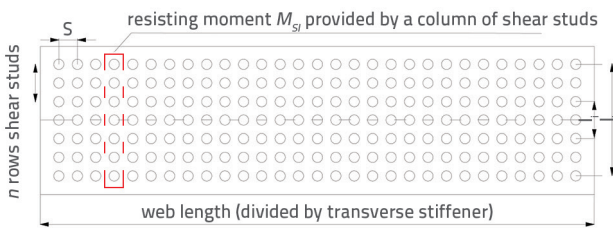

Figure 4. Distribution of shear studs on flange

The average bending moment per unit length along the flange-web joint connections is:

$$\frac{M_{s1}}{s} = -\sum_{i=1}^{n} \frac{EAl_i^2}{2s} \frac{\partial w}{\partial y} \tag{22}$$

where s is the longitudinal distance of the shear studs. Thus, the rate of change of the bending (twisting) moment along the flange-web joint connections is:

$$-\frac{\partial w}{\partial x}\left(\frac{M_{s1}}{s}\right) = -\frac{\partial w}{\partial x}\left(\frac{\partial w}{\partial y} \sum_{i=1}^{n} \frac{EAl_i^2}{2s}\right) \tag{23}$$

From Eq. (3), the rate of change of the twisting moment along the flange-web joint connections in the flange is shown to be numerically equal to the bending moment per unit length of the upper edge of the web and can be expressed as:

$$-D\left(\frac{\partial^2 w}{\partial y^2} + v \frac{\partial^2 w}{\partial x^2}\right) = -\frac{\partial w}{\partial x}\left(\frac{\partial w}{\partial y} \sum_{i=1}^{n} \frac{EAl_i^2}{2s}\right) \tag{24}$$

Which can be simplified as:

$$D \frac{\partial^2 w}{\partial y^2} \approx \frac{\pi}{l} \sum_{i=1}^{n} \frac{EAl_i^2}{2s} \tag{25}$$

Thus, the equivalent torsional rigidity of the flange can be expressed as:

$$C_s = \frac{l}{\pi} \sum_{i=1}^{n} \frac{EAl_i^2}{2s} \tag{26}$$

Substituting the results of Eq. (19) into Eq. (5), the boundary conditions of the rotationally restrained edges in the composite girder are expressed as follows:

$$D \frac{\partial^2 w}{\partial y^2} \approx C_z \frac{\pi^2}{l^2} \frac{\partial w}{\partial y} = \left(C_t + \min\{C_s, C_c\}\right) \frac{\pi^2}{l^2} \frac{\partial w}{\partial y}_{,y=h} \tag{27}$$

Because the torsional rigidity of the concrete deck C_c is much larger than that of the shear studs C_s, the torsional rigidity of the concrete-steel combination flange is determined by the torsional rigidity of the shear studs. The elastic rotationally restrained coefficient of the concrete-steel combination flange (χ_t) is expressed as:

$$X_t \approx \frac{k_t h}{D} = \left(C_t + \sum_{i=1}^{n} \frac{EAl_i^2}{2s\pi}\right) \frac{\pi^2 h}{l^2 D} \tag{28}$$

The elastic rotationally restrained coefficient of the flange without the concrete deck (χ_0) is expressed as:

$$X_0 \approx \frac{k_0 h}{D} = C_0 \frac{\pi^2 h}{l^2 D} \tag{29}$$

Eqs. (28) and (29) show that the elastic rotationally restrained coefficient of the flange-web joint connection is inversely proportional to the square of the web width and is proportional to the depth of the web.

4. Parametric analysis

Based on Timoshenko's Buckling Theory [20], the elastic rotationally restrained coefficient provided by the web-flange joint connections of the concrete-steel combination flange is derived using Eq. (28). Parametric analysis was performed to verify the accuracy of the theoretical model.

4.1. Critical buckling stress solution (stress gradient $\lambda = 0$)

In the case of the stress gradient $\lambda = 0$, assuming that the aspect ratios were 2/3 and 1/1 respectively, the elastic rotationally restrained coefficients ($\chi_0 = \chi_t$) for the upper and lower flanges were increased from 0 to 50, (the restrained coefficient $\chi_0 = \chi_t = 0$ indicates the simply supported edge, and $\chi_0 = \chi_t \to \infty$ indicates the clamping supported edge). The analysis results are shown in Figure 5, which shows that the local critical buckling coefficient increases as the restrained coefficient increases, and when the value of $\chi_0 = \chi_t$ is larger than 20, the growth rate of critical local buckling coefficient k_b will slow down, and the buckling coefficient will tend to remain constant.

Two cases are shown in Figure 6: (1) in which all the edges are simply supported (SSSS) and (2) in which the loading edges are simply supported and the unloading edges are clamp-supported (CCSS). As shown in Figure 6, the results of the model developed in this study are close to the traditional theoretical results [21], with an error rate < 3%.

4.2. Critical buckling stress solution

Figure 7 shows how the stress gradient λ affected the critical buckling coefficient. The relationship curve of the rotationally restrained coefficient and the buckling coefficient for different pressures, where the pressure gradient λ was equal to 0.5, 1.0, and 1.5 respectively, is shown in Figure 7. As the stress gradient λ increases, the buckling coefficient also increases. As shown in Figure 7, the buckling coefficient increases with the restraint coefficient. The relationship of the aspect ratio to the buckling coefficient for the pressure of the stress gradient $\lambda = 2$ is shown in Figure 8. When all web edges were simply supported (SSSS), the loading edges were simply supported, and the unloading edges were clamp-supported (CCSS). The results were compared to those of the traditional theory [21], and the error rate was <3%.
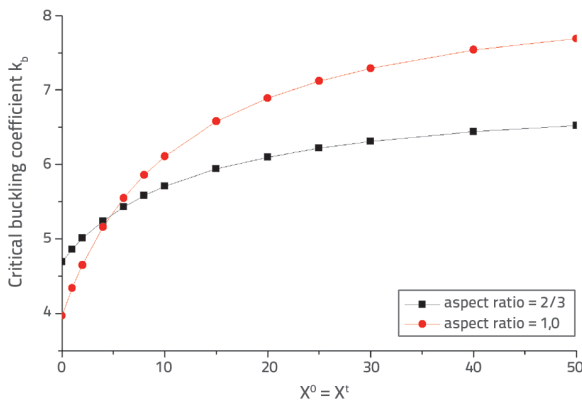

Figure 5. Critical local buckling coefficient of the web when the rotationally restrained coefficients of the upper and lower flanges were changed from 0 to 50 at aspect ratios of 1/1 and 2/3

Figure 7. Relationship of the critical buckling coefficient and the upper and lower rotationally restrained coefficients under uneven pressures, when the stress gradient $\lambda = 0.5$, 1.0, and 1.5 respectively
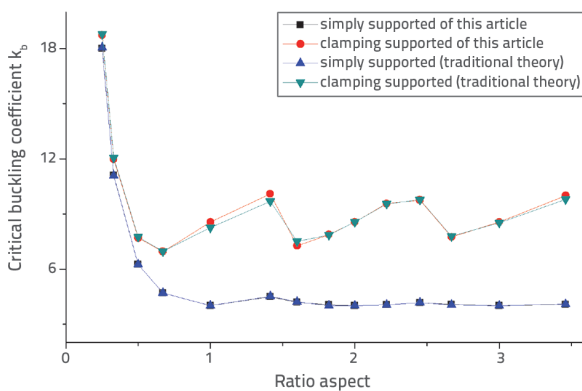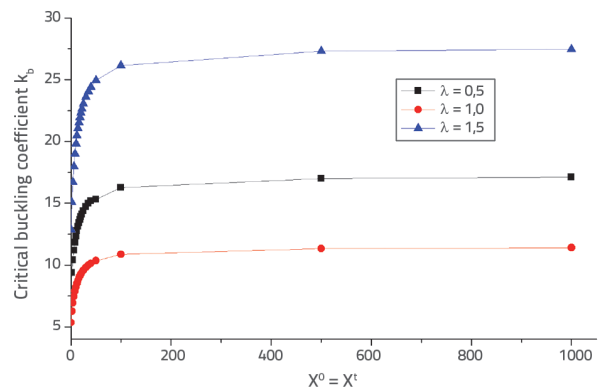

Figure 6. Critical local buckling coefficient when the web was under uniform pressure was compared with that of the traditional model in the literature [21] and with the model developed in this study
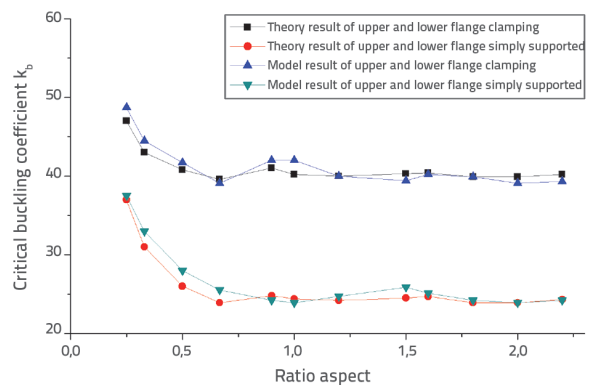

Figure 8. Comparison of the critical local buckling coefficient from the traditional model in the research literature [21] and the model developed by this article with the stress gradient of $\lambda = 2$

5. Numerical analysis

ANSYS, a large-scale universal finite element software, is widely recognised for its calculation results, which can accurately simulate the buckling behaviour of structures under various complex working conditions. Therefore, a numerical analysis was conducted using the finite element software ANSYS 2019 to evaluate the influence of different shear nail distributions on the critical local buckling coefficients of composite beams. The steel plate material was Q370qE, the bolt material was ML15, and the concrete material grade was C55. The material parameters are listed in Table 2. The steel beams were SHELL181 units, the bolts were BEAM188 units, and the concrete was SOLID65 units. The composite girder segments between two adjacent transverse stiffeners were modelled as shown in Figure 9, and the boundary conditions and loading were defined as shown in Figure 10 and Table 3. The flanges and web were modelled separately but were coupled with the degrees of freedom of Rot_x on the nodes of the web-flange joint connections. This geometry was selected to isolate, as much as possible, the behaviour of the web without neglecting the effect of the flanges, with an aspect ratio for the web of 1.0 and a stress gradient of $\lambda = 1$.

ELEMENTS

Figure 9. Finite element model of the composite I-section girder segment

Table 2. Material parameters

Material	Elastic modulus [GPa]	Yield strength [MPa]	Ultimate strength [MPa]	Poisson's ratio
Q370qE	210	370	510	0.3
ML15	210	354	437	0.3
C55	35.5	/	/	0.2

Table 3. Boundary conditions of the FEM (0 and 1 represent the boundary condition clamping, or free)

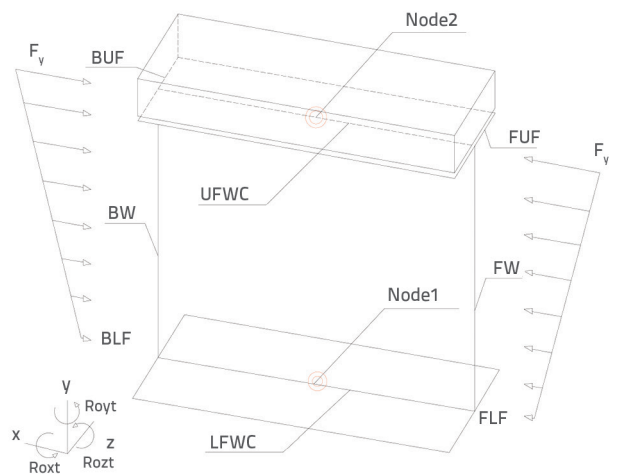| Boundary conditions	u_x	u_y	u_z
BUF (Back upper flange)	0	1	0
BW (Back web)	0	0	1
BLF (Back lower flange)	0	1	0
FUF (Forward upper flange)	0	1	0
FW (Forward web)	0	0	1
FLF (Forward lower flange)	0	1	0
LFWC (Lower flange web connect)	0	0	1
UFWC (upper flange web connect)	0	0	1
Node 1	1	0	1
Node 2	1	0	1

Figure 10. Boundary conditions of web in I-section composite girder obtained by numerical analysis

Table 4. Segment parameters and element type of the finite element model

Element names	Parameters [mm]
Upper flange (shell63)	width × thickness, 1600 × 16
Web (shell63)	width × thickness, 4000 × 20
Lower flange (shell63)	width × thickness, 2000 × 20
Concrete deck (solid45)	width × thickness, 1600 × 600
Shear stud (beam4)	diameter, 10

Table 5. Comparison of FEA and theoretical results

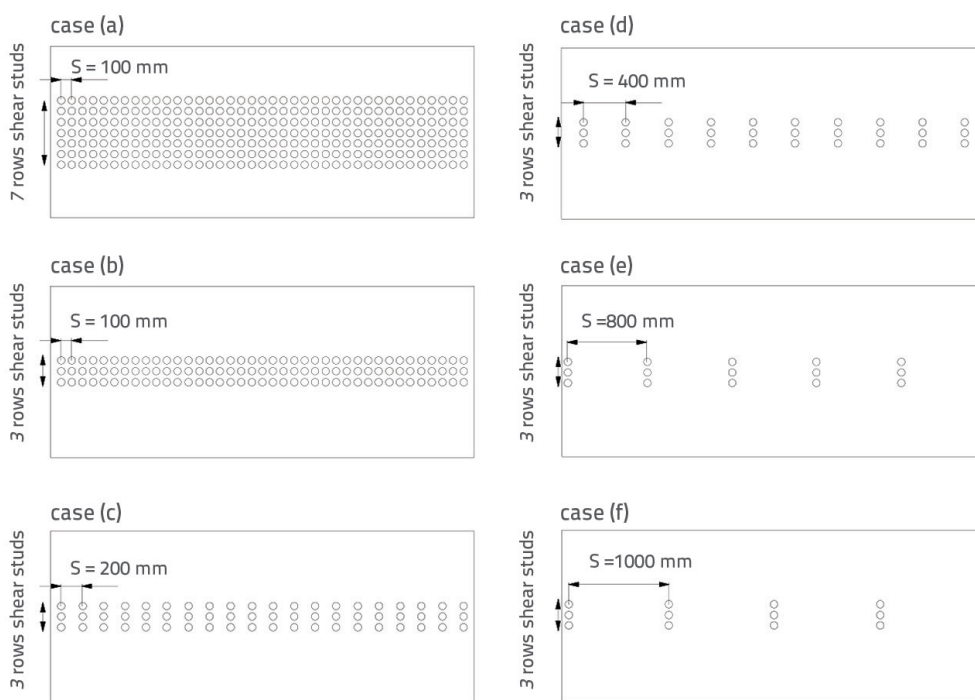| Shear stud distribution	χ_0	χ_t	FEM results [MPa]	This paper results [MPa]	Error [%]
case (a)	7.21	227.16	127.85	135.43	5.92
case (b)	7.21	26.07	121.90	127.13	4.29
case (c)	7.21	13.80	120.51	121.20	0.57
case (d)	7.21	7.66	118.38	114.54	3.24
case (e)	7.21	4.59	114.81	108.53	5.47
case (f)	7.21	3.98	113.29	106.89	5.64
without concrete deck	7.21	1.53	98.69	98.50	0.19

Figure 11. Six cases of shear stud distributions

The model steel-concrete composite girder segment parameters and element types are listed in Table 4. The distances used between the shear studs in Table 4 are only for the convenience of theoretical research and cannot be used as a basis for structural design.

The shear stud distribution was the main variable whose influence was analysed. The shear stud distributions included six cases, as shown in Figure 11. With the in-plane load stress gradient at λ = 1, the resulting web critical local buckling coefficient from the numerical analysis, and theoretical results from Eqs. 17, 28, and 29 are shown in Table 5, and the buckling mode is shown in Figure 12.

As indicated in Table 5 and Figure 13, as the distance of the shear studs increased from 100 to 1000 mm, the elastic rotational coefficient χ_t of the steel-concrete composite flange decreased, and the critical buckling stress σ_{cr} of the numerical simulation results also decreased from 121.90 to 113.29 MPa.

The critical buckling stress of case (a) was close to case (b), due to the fact that the elastic restraint coefficient χ_t, provided by the combination flange from case (a) had passed 20, and the critical local buckling stress tends to remain constant once the elastic restraint coefficient χ has passed 20.
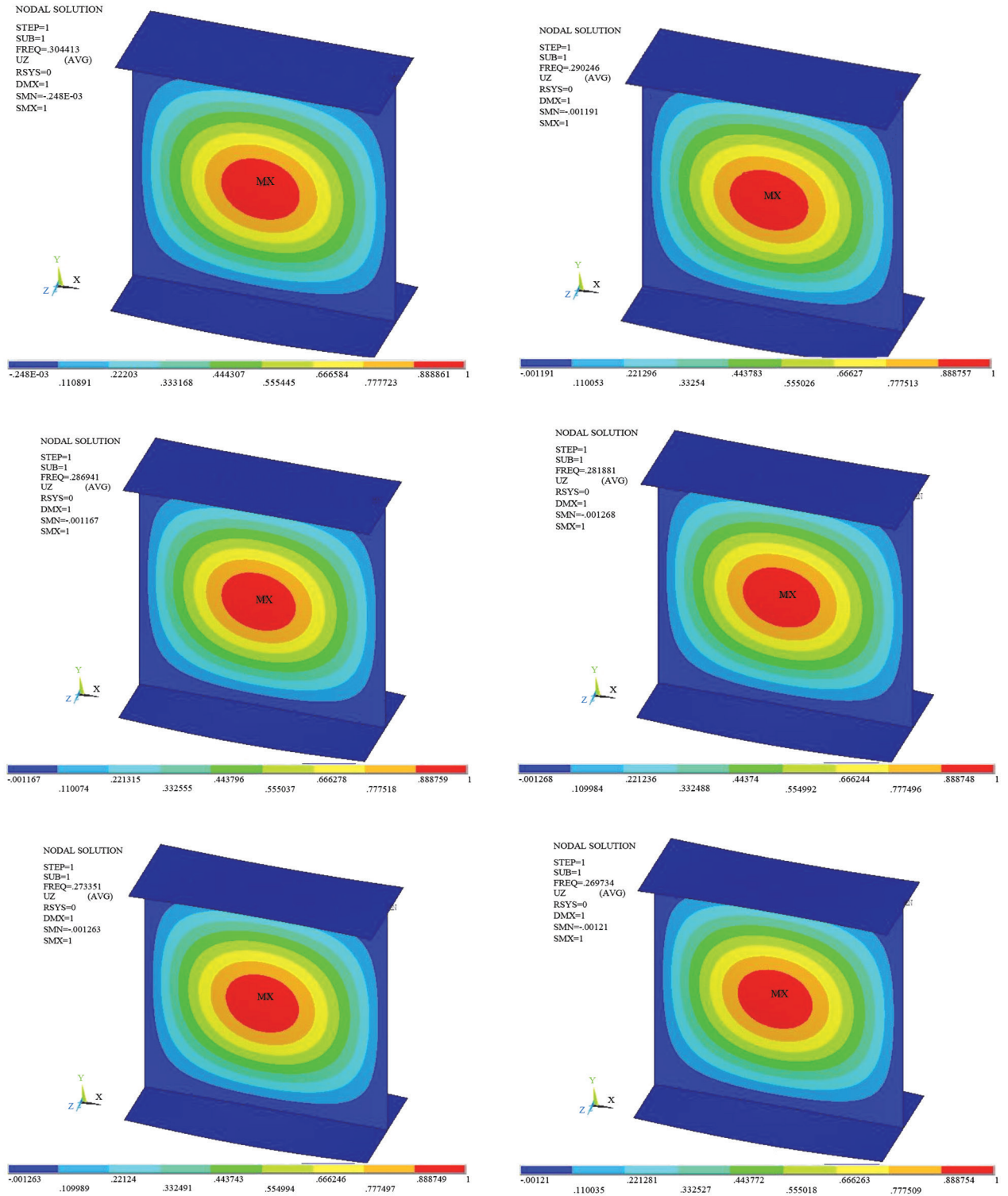
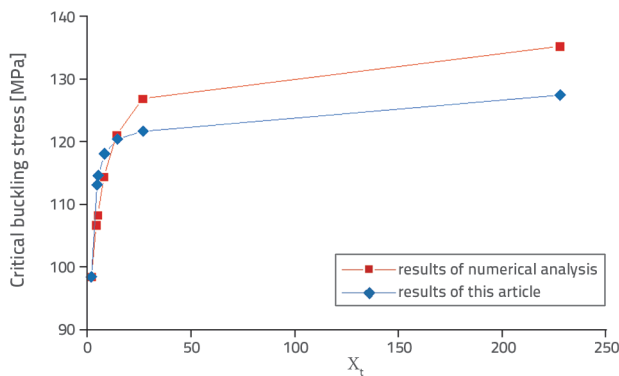Figure 12. Buckling modes for different stud shear distributions

Figure 13. Web critical buckling stress from numerical analysis and this article ($\lambda = 1$)

6. Conclusion

In the theoretical investigation conducted in this study, the buckling behaviour of webs restrained by flanges in steel-concrete composite girders was examined. Based on the Ritz Energy Variational Method and Plate Elastic Buckling Theory, a theoretical solution formula was proposed for the critical local buckling coefficient of web plates under uneven pressure, and a theoretical method was developed to calculate the elastic restraint coefficient of steel-concrete composite flanges with different shear stud distributions. To verify that the theoretical model was correct, a numerical analysis using FEM was performed.

The conclusions are as follows:
- As the distance of the shear studs increased from 100 to 1000 mm, the elastic rotational coefficient χ_t of the steel-concrete composite flange decreased, the critical buckling stress (stress gradient $\lambda = 1$) σ_{cr} of the numerical simulation results also decreased from 121.90 to 113.29 MPa, which coincides with the results of this article, and error rates were < 6%.
- The critical buckling stress in case (a) was similar to that in case (b). The reason for this phenomenon was that the elastic restraint coefficient χ_t provided by the combination flange from case (a) had passed 20, and the critical local buckling stress tends to remain constant once the elastic restraint coefficient χ has passed 20.
- Compared with the values from the traditional theory, the error results of the model developed by this article, under uniform pressure (stress gradient $\lambda \neq 0$) and uneven axial pressure (stress gradient $\lambda \neq 0$), were <3%.
- The elastic rotational coefficient formula of the web in the steel–concrete composite girder developed in this study was sufficiently precise to be used in buckling assessments of webs in composite girders.

Acknowledgements

LITERATURA

[1] Alinia, M.M., Moosavi, S.H.: Stability of longitudinally stiffened web plates under interactive shear and bending forces, Thin-walled Structures, 47 (2009) 1, pp. 53-60, https://doi.org/10.1016/j.tws.2008.05.005

[2] Alinia, M.M., Shakiba, M.: Shear failure characteristics of steel plate girders, Thin-walled Structures, 47 (2009) 12, pp. 1498-1506, https://doi.org/10.1016/j.tws.2009.06.002

[3] Grondin, G.Y., Chen, Q, Elwi, A.E.: Stiffened steel plates under compression and bending, Journal of Constructional Steel Research, 45 (1998) 2, pp. 125-148, https://doi.org/10.1016/S0143-974X(97)00058-8

[4] Wright, H.D.: Local stability of filled and encased steel sections, Journal of Structural Engineering, 121 (1995) 10, https://doi.org/10.1061/(ASCE)0733-9445(1995)121:10(1382)

[5] Yvan, G., Pierre-Olivier, M.: Presentation Manual of EBPlate, Working document COMBRI/CTICM-xx, DRAFT 1, Liege-11 & 12/07/2006.

[6] Estrada, I., Real, E., Mirambell, E.: Shear resistance in stainless steel plate girders with transverse and longitudinal stiffening, Journal of Constructional Steel Research, 64 (2008) 11, pp. 1239-1254, https://doi.org/10.1016/j.jcsr.2008.07.013

[7] Estrada, I., Real, E., Mirambell, E.: A newly developed expression to determine more realistically the shear buckling stress in steel plate structures, Thin-walled Structures, 64 (2008) 7-8, pp. 737-747, https://doi.org/10.1016/j.jcsr.2008.01.028

[8] Poologanathan, K., Mahen, M.: Elastic shear buckling characteristics of LiteSteel beams, Thin-walled Structures, 66 (2010) 11, pp. 1309-1319, https://doi.org/10.1016/j.jcsr.2010.05.005

[9] Bedair, O.K.: Influence of in-plane restraint on the buckling behaviour of plates under uniform compression, shear, and in-plane bending, Computer Methods Applied Mechanics Engineering, 148 (1997) 1-2, pp. 1-10, https://doi.org/10.1016/S0045-7825(97)00035-2

[10] Qiao, P.Z., Zou, G.P.: Local buckling analysis of elastically restrained fibre-reinforced plastic plates and its application to box sections, Journal of Engineering Mechanics, 128 (2002) 12, https://doi.org/10.1061/(ASCE)0733-9399(2002)128:12(1324)

[11] Qiao, P.Z, Shan, L.Y.: Explicit local buckling analysis and design of fiber-reinforced plastic composite structural shapes, Thin-walled Structures, 70 (2005) 4, pp. 468-483, https://doi.org/10.1016/j.compstruct.2004.09.005

[12] Pham, C.H., Hancock, G.J.: Shear buckling of thin-walled channel sections, Journal of Constructional Steel Research, 65 (2009) 3, pp. 578-585, https://doi.org/10.1016/j.jcsr.2008.05.015

[13] Liang, C., Liu, Y., Chen, S., Lu, C.: Study on threshold interfacial shear stiffness of simply supported composite girders, Engineering Structures, 1 (2022) 268, pp.114736, https://doi.org/10.1016/j.engstruct.2022.114736

[14] Rossi, A., Nicoletti, R.S., de Souza, A.S., Martins, C.H.: Numerical assessment of lateral distortional buckling in steel-concrete composite beams, Journal of Constructional Steel Research, 1 (2020) 172, pp. 106192, https://doi.org/10.1016/j.jcsr.2020.106192

[15] Śledziewski, K., Górecki, M.: Finite element analysis of the stability of a sinusoidal web in steel and composite steel-concrete girders. Materials, 26 (2020) 13, pp.1041, https://doi.org/10.3390/ma13051041

[16] Wijethunge, W.M., Dammika, A.J., Bandara, C.S., Jayasinghe, J.A.: Three-dimensional numerical simulation of lateral distortional buckling behaviour of steel–concrete composite beams, Engineer, 56 (2023) 2, pp. 23-35. https://doi.org/10.4038/engineer.v56i2.7574

[17] Araujo, H.F., Andrade Jr., C.M., Basaglia, C., Camotim, D.: Lateral-distortional buckling of steel-concrete composite beams: kinematics, constrained-mode GBT, and analytical formulae, Journal of Constructional Steel Research, 192 (2022), pp. 107210, https://doi.org/10.1016/j.jcsr.2022.107210

[18] László, P.K.: Local Buckling of Fibre Reinforced Plastic Composite Structural Members with Open and Closed Cross Sections, Journal of Structure Engineering, 129 (2003)11, p. 1503, https://doi.org/10.1061/(ASCE)0733-9445(2003)129:11(1503)

[19] László, P.K.: Buckling of Unidirectionally Loaded Composite Plates with One Free and One Rotationally Restrained Unloaded Edge, Journal of Structure Engineering, 128 (2002) 9, pp. 1202-1211, https://doi.org/10.1061/(ASCE)0733-9445(2002)128:9(1202)

[20] Timoshenko, S.: Theory of Elastic Stability, McGraw Hill, New York, 1965.

[21] Chen, J.: Stability of Steel Structures Theory and Design, Science Press, Beijing, China, 2008.